

# We are IntechOpen, the world's leading publisher of Open Access books Built by scientists, for scientists

**6,900**

Open access books available

**186,000**

International authors and editors

**200M**

Downloads

**154**

Countries delivered to

**TOP 1%**

most cited scientists

**12.2%**

Contributors from top 500 universities



**WEB OF SCIENCE™**

Selection of our books indexed in the Book Citation Index  
in Web of Science™ Core Collection (BKCI)

Interested in publishing with us?  
Contact [book.department@intechopen.com](mailto:book.department@intechopen.com)

Numbers displayed above are based on latest data collected.

For more information visit [www.intechopen.com](http://www.intechopen.com)



## Chapter

# High Precision Optical Wavefront Generation Using Liquid Crystal Spatial Light Modulator (LC-SLM)

Zixin Zhao

## Abstract

LC-SLM provides a flexible way to modulate the phase of light with the help of a grayscale pattern loaded on it. Nevertheless, the modulated phase profile is of relatively low accuracy due to the nonlinear and nonuniform response of the liquid crystal layer in the SLM. To improve the performance of LC-SLM on the wavefront generation, the nonlinear and nonuniform phase response needs to be calibrated and compensated effectively. In this chapter, we present some state-of-art methods to measure the phase modulation curve of the LC-SLM. Some methods to measure the static aberration caused by the backplane of the LC-SLM are then presented. Last but not the least, the future development of the LC-SLM in phase modulation is also presented.

**Keywords:** liquid crystal spatial light modulator, phase calibration, wavefront generation, interferometry

## 1. Introduction

A spatial light modulator is a device that modulates the spatial distribution of light waves. Generally speaking, the spatial light modulator is composed of many independent units, which are arranged into one-dimensional or two-dimensional array structures in space. Each unit independently receives the control of optical signal or electrical signal, and changes the amplitude or intensity, phase, and polarization of light received in space. Because of the excellent properties of liquid crystal, liquid crystal spatial light modulator (LC-SLM) is widely used in adaptive optics [1], diffractive optical elements [2], optical testing [3], and so on [4].

According to the different addressing modes of the spatial light modulator, it can be divided into electrical addressing spatial light modulator (EA-SLM) and optical addressing spatial light modulator (OA-SLM). The electrically addressable spatial light modulator usually adds the signal to the corresponding unit through two groups of orthogonal grid electrodes on the SLM by means of progressive scanning. The input signal of the optically addressable spatial light modulator is an optical signal, which can convert the intensity distribution of writing light into charge distribution, refractive index distribution, and so on. In recent years, due to the rapid developments of liquid crystal display and VLSI technology and the abundance of liquid crystal materials, the application of electrically addressable liquid crystal spatial light modulators as wavefront correction devices in adaptive optics

has attracted more and more attention. As a result, electrically addressable LC-SLM has great potential in realizing high-resolution wavefront control of optical systems.

The typical structure of a reflective LC-SLM is shown in **Figure 1**. It looks like a “sandwich” with three parts. The upper part is the covering glass with a transparent conductive film. The middle part is a liquid crystal layer containing thousands of liquid crystal molecules. And the bottom part is the silicon substrate containing discontinuous reflection pixels.

When the voltage is applied, the molecular structure of the liquid crystal will twist, resulting in the change of the birefringence coefficient of the liquid crystal. This electro-optic effect is called the electrically controlled birefringence effect. The electric field makes the liquid crystal molecules polarized and deflected, and changes the arrangement of liquid crystal molecules. With the increase of voltage, the liquid crystal molecules will break away from the intermolecular attraction and gradually incline along the electric field. When the threshold voltage is exceeded, except for the surface viscous force at the electrode substrate, other liquid crystal molecules will rearrange along the electric field direction. Different phase modulation can be generated by controlling the liquid crystal voltage, as shown in **Figure 1**. The phase delay between extraordinary light (*e* light) and ordinary light (*o* light) is shown in Eq. (1).

$$\delta = \frac{4\pi}{\lambda} \int_0^d (n_e(\theta) - n_o) dz \quad (1)$$

where  $d$  is the thickness of the liquid crystal layer, and  $n_e(\theta)$  represents the refractive index of extraordinary light and can be expressed by Eq. (2).

$$n_e(\theta) = \frac{n_e \cdot n_o}{\sqrt{n_e \sin^2 \theta + n_o \cos^2 \theta}} \quad (2)$$

where the deflection angle  $\theta$  is related to the applied voltage and can be expressed by Eq. (3).

$$\theta = \begin{cases} 0 & V \leq V_C \\ \frac{\pi}{2} - 2 \tan^{-1} \left\{ \exp \left[ - \left( \frac{V - V_C}{V_0} \right) \right] \right\} & V > V_C \end{cases} \quad (3)$$

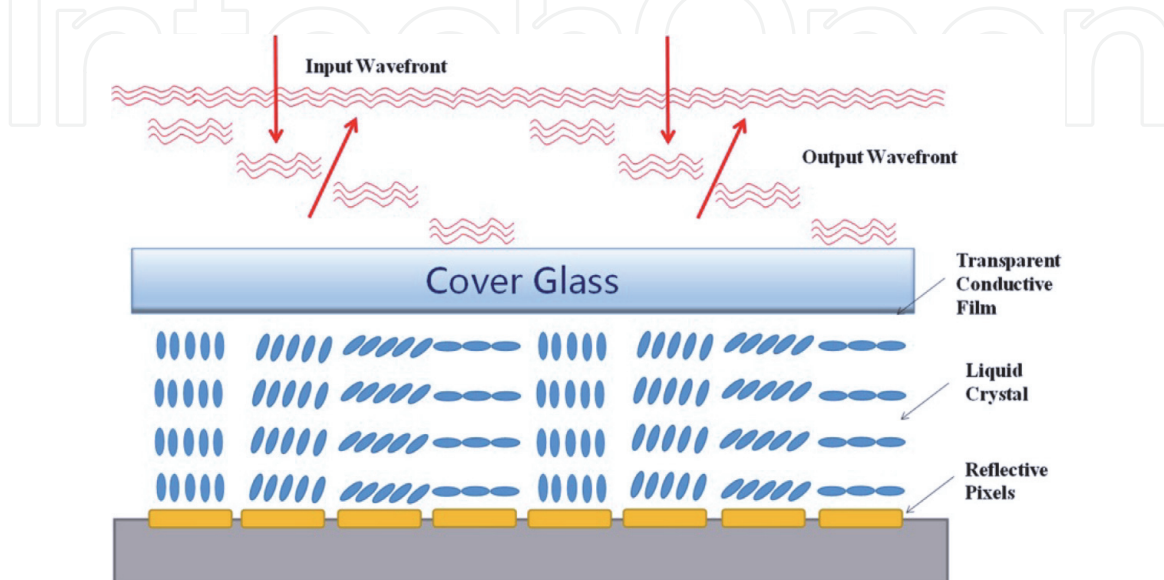


**Figure 1.**  
Typical structure of a reflective LC-SLM.

where  $V_c$  is the initial voltage of the liquid crystal molecule when it starts to deflect, namely the threshold voltage. Therefore, the phase modulation produced by the electronic birefringence is related to the voltage applied at both ends of the liquid crystal layer.

It can be clearly seen from Eq. (3) that the relationship between the deflection angle and the applied voltage is nonlinear. As a result, the phase response of the LC-SLM is nonlinear, which needs to be calibrated accurately.

## 2. Nonlinear phase response calibration

### 2.1 Traditional methods to measure the phase modulation curve of LC-SLM

The phase response calibration is to measure the phase modulation curve with respect to the applied voltage (grayscale). In general, the measurement methods of phase modulation characteristics can be divided into two groups—the interference method and the diffraction method. Among them, interferometry mainly includes double-slit/hole interferometry [5–7], Twyman-Green interferometry [8–11], Mach-Zehnder interferometry [12–14], and digital holographic interferometry [15–17]. The measurement of phase modulation characteristics of interferometry mainly depends on the displacement of fringe pattern, but the two beams have to travel a long path in the air before the interference, and the mechanical vibration, air turbulence, and other environmental factors will cause the change of their optical path difference, resulting in a large fluctuation in the acquisition of fringe pattern. Diffraction methods are mainly based on irradiance measurements of the diffraction pattern originated by phase holograms at their focal planes [18–21]. Intensity transmission can well suppress the influence of environmental vibration and air turbulence, but from the perspective of phase extraction, the operation process of phase estimation is more complex. Here, we mainly introduce some commonly used calibration methods.

#### 2.1.1 Diffraction-based methods

**Figure 2** shows a typical configuration for phase modulation measurement based on the diffraction of the loaded phase hologram. After beam expansion and

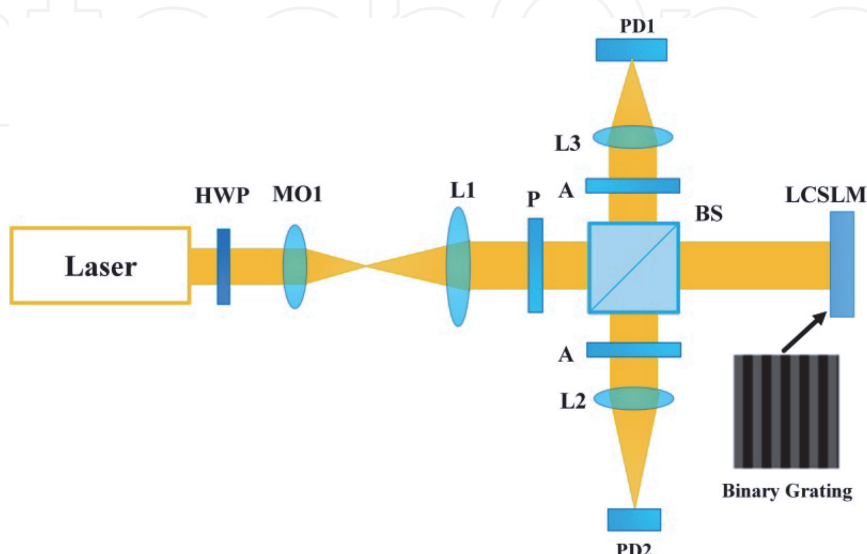


**Figure 2.**  
Schematic of the diffraction-based method by using a binary grating. HWP—half waveplate, MO—micro objective, L1, L2—lens, P—polarizer, A—analyzer, PD1, PD2—photodiode.

collimation, the polarized plane wave is divided into two beams by the beam splitter (BS). One beam of light is detected by the first photodiode (PD1), which is used for the correction of any power jitter. Another beam is reflected by LC-SLM where a binary grating is loaded. And the first diffraction order light of the grating is detected by the second photodiode (PD2). According to the Fourier optics theory [22], the diffraction efficiency of the binary grating is related to the phase difference of the two levels. As a result, by changing the phase difference of the loaded two-level grating, the phase modulation value can be calculated from Eq. (4) [19].

$$\delta = \sin^{-1} \frac{\pi}{2} \sqrt{\frac{P_2}{P_1}} \quad (4)$$

where  $P_1$  and  $P_2$  represent the intensity detected by the PD1 and PD2, respectively. Note that the optical system shown in **Figure 2** is somewhat complex. To simplify the system, a circular grating (binary Fresnel phase lens) [20] was adopted instead of a linear grating. Due to the use of circular grating, the physical lens is no longer needed and the use of minimal optical elements allows a fast alignment of the experimental setup as shown in **Figure 3**. This compact configuration makes it suitable for *in situ* calibration for SLM.

### 2.1.2 Interferometry-based methods

Different from the diffraction-based methods where the phase response is characterized by the first-order diffraction efficiency of the loaded binary grating, the interferometry-based methods utilized the movement of the interference fringe to calculate the phase shift value. The first commonly used interferometric method is the double-slit/hole interferometry whose optical setup is shown in **Figure 4**.

After the laser passes through the half-wave plate (HWP), it forms a plane wave through the beam expansion collimation system composed of micro-objective lens (MO1) and lens (L1). Then, it needs to travel through the polarizer (P) and the mask with two holes (or slits) placed in front of the LC-SLM. At this time, the parallel light is divided into two beams by mask and incident on the target surface of LC-SLM, respectively. The gray image loaded into LC-SLM consists of two equal parts, one of which has a constant gray value of 0, and the other increases gradually from 0 to 255. Then, the two beams modulated by LC-SLM are focused by lens L2 and amplified by MO2. The interference fringes of the two beams are recorded by CCD. The double-slit/hole interferometry belongs to the common path interferometry, which is not easy to be interfered by the environmental turbulences, but the interference only occurs in the light transmission area of the mask, so the measured results can only reflect the modulation results of the local range of the target

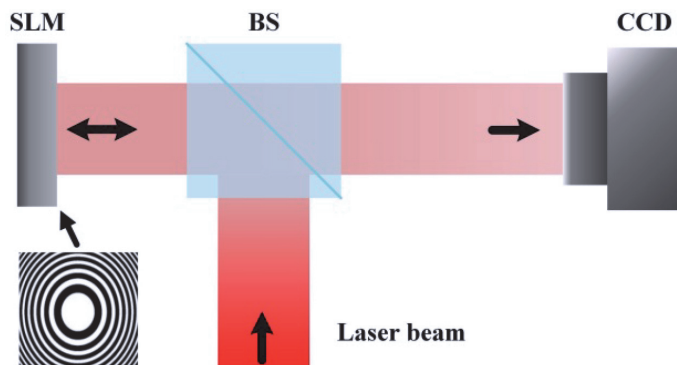


**Figure 3.**  
Simplified setup of the diffraction-based method by using a binary circular grating [20].

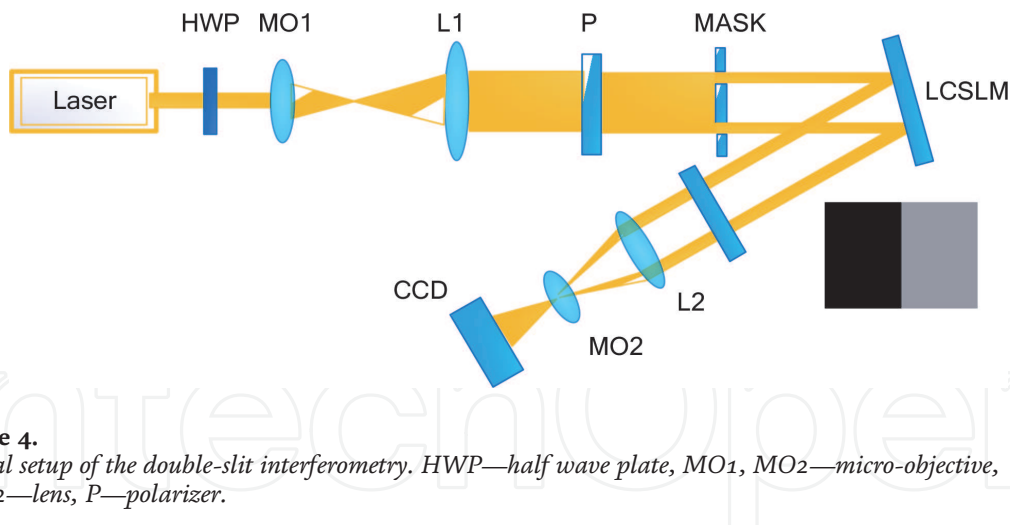


**Figure 4.**

Optical setup of the double-slit interferometry. HWP—half wave plate, MO<sub>1</sub>, MO<sub>2</sub>—micro-objective, L<sub>1</sub>, L<sub>2</sub>—lens, P—polarizer.

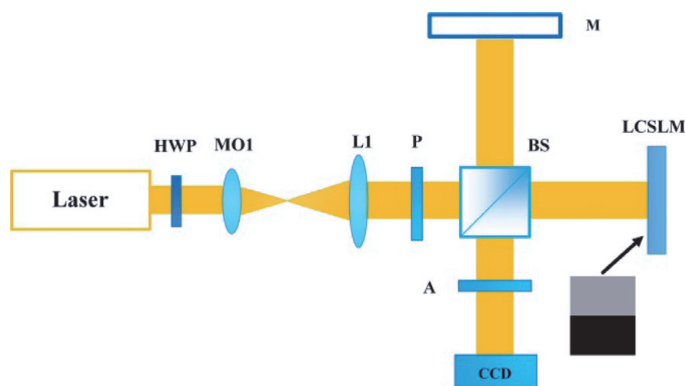


**Figure 5.**

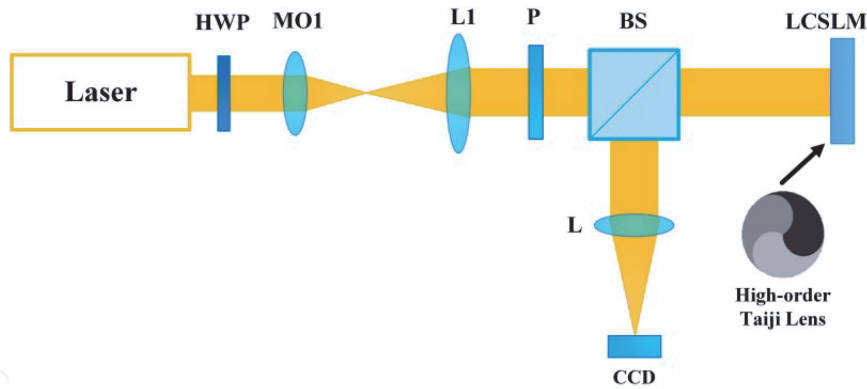
Optical layout of the Twyman-Green interferometry. HWP—half waveplate, MO<sub>1</sub>—micro-objective, L<sub>1</sub>—lens, P—polarizer, A—analyzer, M—mirror.

surface, and cannot accurately detect the phase modulation characteristics of the whole working surface. Recently, some researchers [23] used the SLM itself to generate the double holes so that the physical aperture with two holes is no longer needed. Since the calibration area is more easily adjusted, it can be used in different experimental conditions. As a matter of fact, if the double-slit/hole (mask) is replaced by a grating [24], the first-order diffracted beams can also interfere after passing the lens. However, the zero-order light needs to be blocked out so as to get an interference fringe pattern with a good contrast.

Another commonly used method is the Twyman-Green interferometry, whose optical layout is shown in **Figure 5**.

After beam expansion and collimation, the plane wave is divided into two beams by the beam splitter (BS). One beam of light is perpendicular to LC-SLM and reflected after modulation by LC-SLM with loading grayscale image. The modulated light then interferes with the light reflected by the plane mirror (M). A CCD is used to record the interference fringes, and the phase modulation curve of LC-SLM is obtained by calculating the relative fringe movement over the fringe period. The results obtained by using the Twyman-Green interferometric method can detect the phase modulation characteristics of the whole working area. However, the two beams travel different paths before they can interfere. As a result, the method is greatly affected by the ambient vibration and air turbulence, which easily causes the fringe jitter and affects the measurement accuracy.

Recently, a radial shear interferometry was proposed by sending a Chinese high-order Taiji lens onto SLM [25]. The optical setup is shown in **Figure 6**. The method is realized by rotating multiple airy points, which are generated by the radial shear

**Figure 6.**

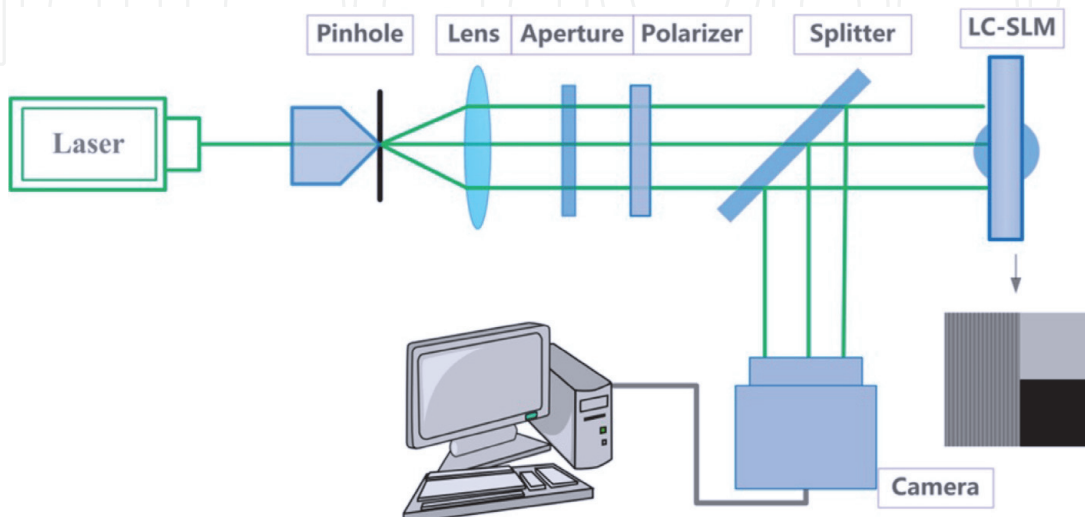
Optical setup of the radial shear interferometry [25]. HWP—half waveplate, MO1—micro-objective, L<sub>1</sub>, L<sub>2</sub>—lens, P—polarizer, A—analyzer.

interference of high-order Chinese Taiji lens. As a result, the phase modulation value is related to the rotation angle of the captured image by CCD. However, the phase shift estimation is highly dependent on the accurate centroid location of the two Airy spots.

## 2.2 Measuring the phase modulation curve of LC-SLM using the self-interference method

As mentioned above, the movement of the interference fringe is used to measure the phase modulation value in the interferometry-based methods. Different phase patterns loaded onto SLM will generate different kinds of interferograms. Inspired by the method in Ref. [26], we propose a self-interference method by using a diffraction grating [27]. The optical layout of the self-interference method is shown in **Figure 7**.

As it can be seen in **Figure 7**, the collimation beams perpendicularly strike the SLM and a beam splitter was used to deflect the reflected beams to the CCD plane. The combined gray pattern loaded on LC-SLM is divided into three parts. The left side is LC-SLM blazed grating with a period of 16 pixels, and the right side is divided into upper and lower parts. The lower part of the gray is zero and remains unchanged in the measurement process, which is called the reference part. In addition, the gray level of the upper part gradually increases from 0 to 255 in 8 steps, which is called the test part. After the reflection of LC-SLM, the first-order

**Figure 7.**

Optical layout of the self-interference method [27].

diffraction light and the left zero-order diffraction light of blazed grating interfere with LC-SLM at a certain distance, resulting in dislocation fringes. With the change of gray level in the right upper part, a series of fringe patterns with different shearing displacements could be obtained. The phase modulation value could then be calculated by using only one interferogram. As a result, the self-interference method can reduce the effect of environmental vibration or air turbulence and improve the measurement precision.

### 2.3 Phase calibration result

The captured fringe pattern is shown in **Figure 8(a)**. Note that light is diffracted vertically from the sharp edge between the uniform grayscale zones, which causes unwanted effects in the fringe pattern. To reduce the diffraction effect, only a small part of the original fringe pattern (as shown in **Figure 8(b)**) was used to calculate the phase shift values. As shown in **Figure 8(b)**, the fringes passing through the red scan line represented the measuring area, and the fringes passing through the blue scan line represented the reference area. The blue line reference area can be expressed as

$$i_1(x) = a(x) + b(x) \cos [2\pi f_x x + \varphi_0] \quad (5)$$

where  $a(x)$  is the background intensity,  $b(x)$  is the modulation depth,  $f_x$  is the spatial carrier frequency of the  $x$  direction,  $\varphi_0$  is the initial phase of the blue reference area fringe. The red line measurement area can be expressed as

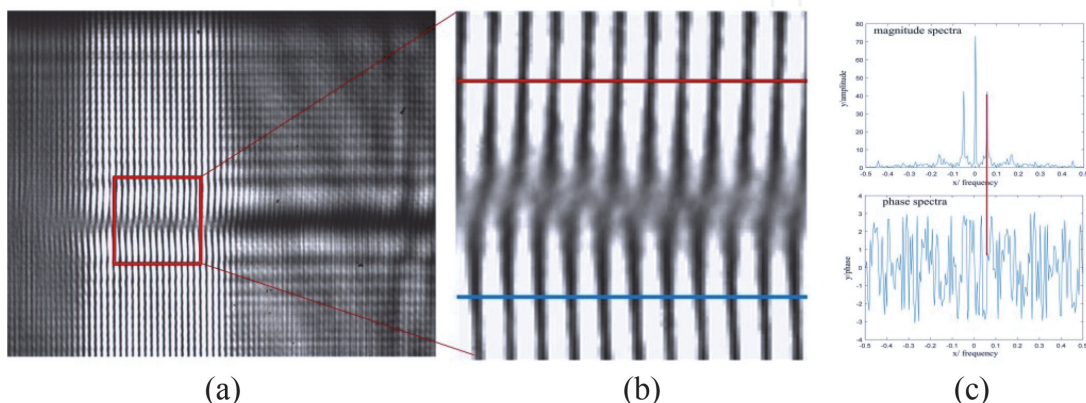
$$i_2(x) = a(x) + b(x) \cos [2\pi f_x x + \varphi_0 + \xi] \quad (6)$$

where  $\xi$  is the amount of phase shift between the measurement area and the reference area. The interference fringes given in Eqs. (5) and (6) are subjected to a Fourier transform:

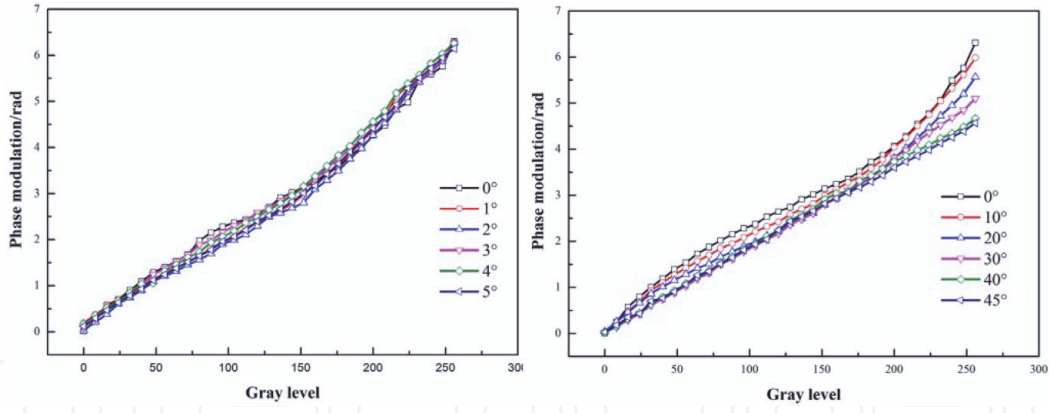
$$F(f) = \int_{-\infty}^{\infty} i(x) \exp(-2\pi jfx) dx \quad (7)$$

where  $j = \sqrt{-1}$ . Then, we can extract the first-order spectrum and obtain its inverse Fourier transform:

$$i_{11}(x) = \int_{-\infty}^{\infty} F(f) \exp(2\pi jfx) df = c(x) \exp\{j[2\pi f_x x + \varphi_0]\} \quad (8)$$



**Figure 8.**  
 Calculating the phase shift using the Fourier transform: (a) the original fringe pattern, (b) the extracted fringe pattern denoted by reading rectangle, and (c) the FFT result of one row in (b).

**Figure 9.**

Phase modulation curves with different incident angles.

$$i_{21}(x) = \int_{-\infty}^{\infty} F(f) \exp(2\pi jfx) df = c(x) \exp \{ j[2\pi f_x x + \varphi_0 + \xi] \} \quad (9)$$

where  $c(x) = \frac{1}{2}b(x)$

$$2\pi f_x x + \varphi_0 = \arctan \frac{\text{Im}[i_{11}(x)]}{\text{Re}[i_{11}(x)]} \quad (10)$$

$$2\pi f_x x + \varphi_0 + \xi = \arctan \frac{\text{Im}[i_{21}(x)]}{\text{Re}[i_{21}(x)]} \quad (11)$$

Finally, the phase shift  $\xi$  is calculated by subtracting Eq. (11) from (10):

$$\xi = \arctan \frac{\text{Im}[i_{21}(x)]}{\text{Re}[i_{21}(x)]} - \arctan \frac{\text{Im}[i_{11}(x)]}{\text{Re}[i_{11}(x)]} \quad (12)$$

The phase modulation was calculated by subtracting the phase of the two side lobes in the frequency domain shown in **Figure 8(c)**. As a result, the relative phase shift of the upper and lower fringes can be obtained by Fourier transform phase analysis. In the actual calculation, 30 rows of data were used in one interferogram and 15 phase modulation values could be obtained. The final phase shift result is the average of these 15 values.

**Figure 9** shows the phase modulation curves of a commercial SLM with different incident angles. It can be seen that the curves are almost coincident when the incident angle is less than 5 degrees, which indicates that the influence of the incident angle on the phase modulation is negligible when the angle is quite small. As the incident angle increases, the phase modulation curves become different. Particularly for the large gray level, their difference is very significant. As a result, the phase modulation depth decreases with the increase of the incident angle when it is larger than 10 degrees. To guarantee a good phase modulation capability, the incident angle is recommended to be less than 5 degrees in practical applications.

### 3. Static aberration measurement and compensation

Generally speaking, reflective LC-SLMs are more widely used in phase-only modulation, compared with transmissive LC-SLMs. The reason is that the reflective structure allows the incident light beam to travel the LC layer twice to obtain a double modulation depth. However, the static aberration of reflective silicon

substrate or backplane, which is caused by the limitations in the polishing process at silicon foundries, leads to the uneven spatial response of SLM. To solve this problem and ensure the phase modulate precision of reflective LC-SLM, it is necessary to accurately measure and compensate the static aberration.

In recent years, several methods have been proposed to fulfill this task. These methods can also be divided into two categories—the diffraction-based methods and the interferometry-based methods. In the former category, the static aberration can be measured by applying a commercial wavefront sensor [28] or utilizing a phase retrieval technique [29–31]. The commercial wavefront sensor such as Shack-Hartman can only obtain a rough estimate of the static aberration. Compared with using a commercial wavefront sensor, the static aberration reconstructed by the phase retrieval technique is more accurate. However, the corresponding time consuming is higher due to the unavoidable iteration process, and the pixel cross talk effect impacts the accuracy of retrieval results as well. In practice, the methods of the latter category, interferometry-based methods, are more widely applied. In the latter category, typically a Michelson interferometer is used to capture the fringe pattern of the static aberration [32–38]. Furthermore, the fringe pattern can be demodulated to obtain the final true phase of aberration, by utilizing the phase-shift technology. Xun and Cohn [39] used the four-step method to demodulating the four interferograms with a phase step of  $\pi/2$ . Later, Arias and Castaneda [38] measured the aberration of an LC-SLM by using Hariharan's five-step method. In their methods, the phase shift is introduced by a mechanical piezo-electric actuator, which is coupled to the reference mirror. Besides, Gongjian et al. [40] utilized the polarization phase-shifting technique to measure the static aberration of SLM. Here, we briefly introduce some recently reported methods.

### 3.1 Diffraction-based methods

A typically diffraction-based method is shown in **Figure 10**. By loading a random phase pattern onto SLM, the corresponding far-field diffraction pattern is captured by CCD. Then, an iterative phase retrieval technique is adopted to estimate the smooth aberration of the SLM [30]. Note that the pixel cross talk should be considered in the iteration process and this effect could be alleviated by using a random phase pattern with a larger feature size. Nevertheless, the measurement accuracy is still limited. Later, ptychography, as shown in **Figure 11**, was proposed to measure the static aberration by moving the SLM with a two-dimensional stage in a later direction [41]. Although the ptychography-based method can get a satisfactory result, the time efficiency is not very high. As a result, the interferometry-based methods are more widely used in the real application.

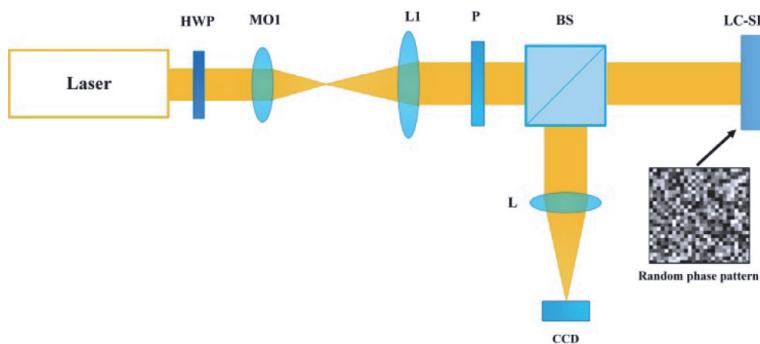


**Figure 10.**  
Optical setup of the static aberration measurement based on iterative phase retrieval [30]. HWP—half waveplate, MOI—micro-objective, L<sub>1</sub>, L<sub>2</sub>—lens, P—polarizer.

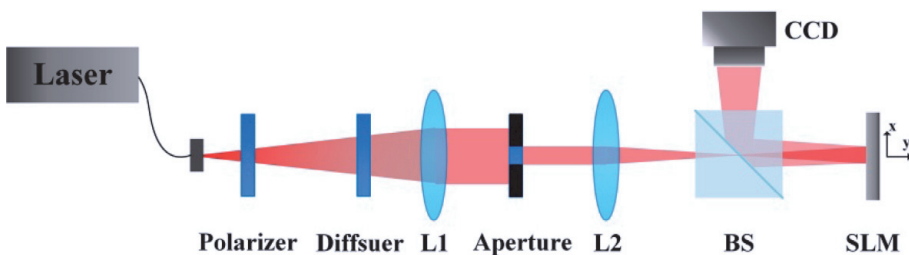


**Figure 11.**  
Optical layout of the static aberration measurement based on ptychography [41].

### 3.2 Interferometry-based method using random phase-shifting technique

Different from the traditional methods, here we introduce a novel interferometry-based method where the arbitrary phase shift is realized by the SLM itself [42]. And the phase is demodulated by a random phase-shifting technique. The configuration is quite simple and can be easily integrated into the optical system where SLM is used. The experimental schematic for this method is shown in **Figure 12**.

A coherent light source with a wavelength of 632.8 nm is generated from the He-Ne laser. After passing through the attenuator, polarizer, spatial filter, and convex lens, a polarized collimated beam is obtained. Note that the polarization angle of the polarizer is set to be consistent with the modulation direction of SLM to ensure a pure phase modulation. The collimated beam is then divided into two parts by the beam splitter. One is the reference beam reflected by the mirror. The other is the test beam modulated by the SLM. These two beams interfere at the splitting surface of the splitter and the corresponding fringe pattern can be captured by the CCD. In addition, the phase shift is achieved by loading different images with the spatially consistent grayscale on the SLM. It should be noted that the mechanical phase shifter is no longer needed, which makes this configuration much simpler and more compact than traditionally used ones.

To show the validity of the introduced compensation method, the static aberration of a SLM (UPOLabs, HDSLM80R) is calibrated. **Figure 13(a-d)** show four

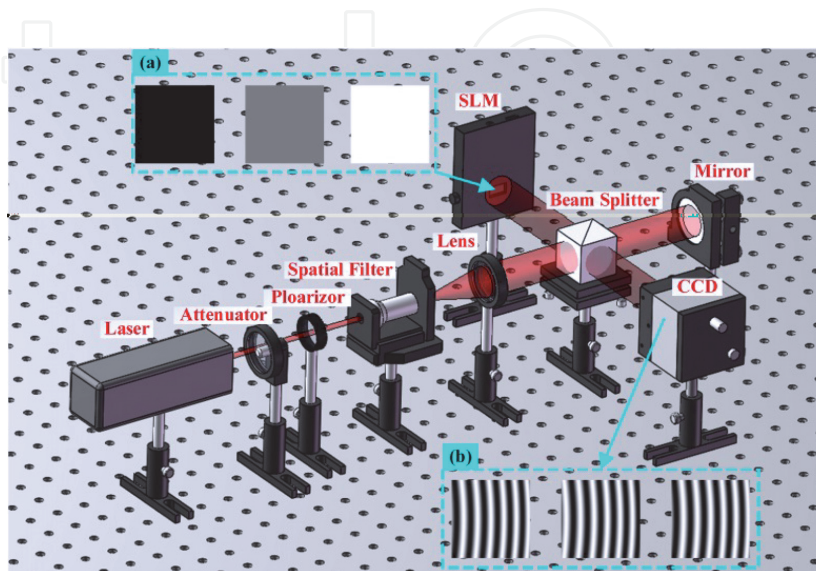


**Figure 12.**  
Experimental schematic for the static aberration measurement based on random phase-shifting interferometry [42]. (a) Constant grayscale patterns loaded on the SLM and (b) the corresponding fringe patterns captured by CCD.

images whose intensity is spatially consistent of 0, 63, 127, and 191, respectively. These images are loaded on the SLM to generate phase shifts, and then, CCD is able to capture four interference fringe patterns, as shown in **Figure 13(e-h)**, respectively. These fringe patterns are demodulated by the VU factorization algorithm [43] and then unwrapped by the derivative Zernike polynomial fitting technique (DZPT) [44]. **Figure 13(i)** and **(j)** show the corresponding demodulated phase map and unwrapped phase map, respectively. Note that the unwrapped phase map is tilt-removed because the first three fitting coefficients of the Zernike polynomial are eliminated in the unwrapping process. Besides, **Figure 13(k)** shows the compensation image used to calibrate the static aberration. This compensation image is calculated by

$$I(x,y) = \frac{255(\mathcal{W}(\psi(x,y)) + \pi)}{2\pi} \quad (13)$$

where  $\psi(x,y)$  represents the tilt removed true phase map, and  $I(x,y)$  is the compensation image needed to be loaded on SLM. After compensation, the interference image captured by CCD is shown in **Figure 13(l)**. It can be seen from **Figure 13(h)** that the fringe pattern only contains some straight fringes

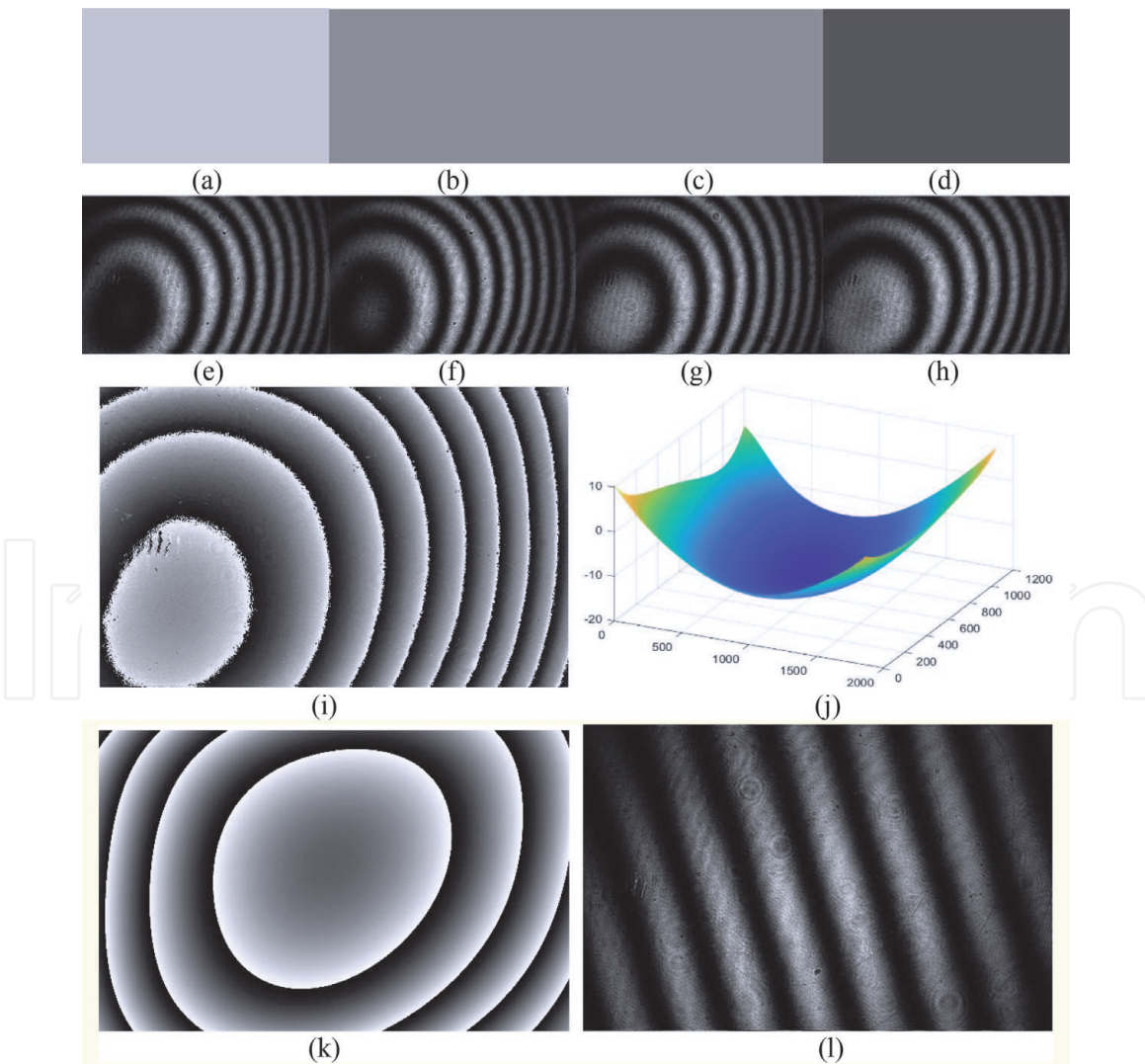


**Figure 13.**  
 Experimental result of the proposed method; (a-d) four phase shift images with the intensity of 0, 63, 127, and 191, respectively; (e-h) four-step fringe patterns of static aberration with random phase shift; (i) demodulated phase map calculated by VU; (j) true phase map calculated by DZPT; (k) compensation phase map for SLM; (l) fringe pattern after compensation.

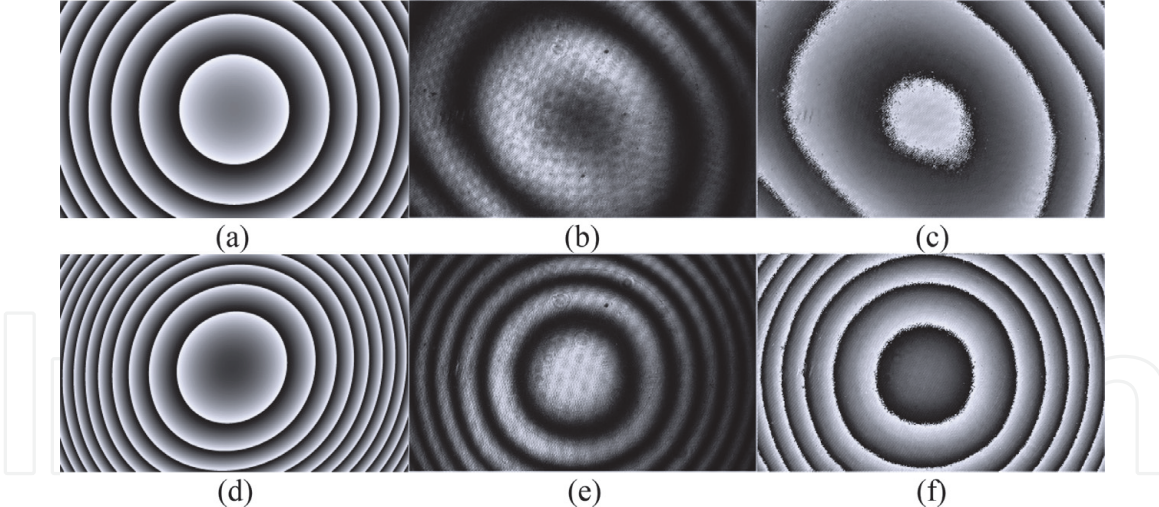


**Figure 14.** Spherical wavefront reconstruction results (a–c) without and (d–f) with static aberration compensation; (a) and (d) are grayscale images to be loaded on SLM; (b) and (e) are fringe patterns captured by CCD; (c) and (f) are demodulated phase maps by VU method [43].

corresponding to the tilt of the reference mirror or SLM, which verifies the effectiveness of the proposed method.

Furthermore, the validity of static aberration compensation results is verified by modulating a circular phase map. This phase map can be modeled as  $\phi_{circular} = 10\pi(x^2 + y^2)$  where  $x \in [-1, 1]$  and  $y \in [-1200/1980, 1200/1980]$ , and its wrapped phase map is shown in **Figure 14(a)**. Without static aberration compensation, the circular phase map is firstly modulated by loading its wrapped phase maps on SLM directly. It should be mentioned that the phase shift is realized by wrapping  $\phi_{circular}$ ,  $\phi_{circular} + 0.5\pi$ ,  $\phi_{circular} + \pi$ , and  $\phi_{circular} + 1.5\pi$ , respectively. **Figure 14(b)** shows one of the fringe patterns captured by CCD, and the corresponding demodulated phase map is shown in **Figure 14(c)**. It can be seen from **Figure 14(b)** and (c) that the phase modulated by SLM has large distortion since the demodulated result deviates from a spherical phase profile. For comparison, the circular phase map is modulated after static aberration compensation as well. To do this, the wrapped phase maps  $\mathcal{W}(\psi + \phi_{circular})$ ,  $\mathcal{W}(\psi + \phi_{circular} + 0.5\pi)$ ,  $\mathcal{W}(\psi + \phi_{circular} + \pi)$ , and  $\mathcal{W}(\psi + \phi_{circular} + 1.5\pi)$  are generated and loaded on SLM. **Figure 14(d)** and (e) show one of the wrapped phase maps and its corresponding fringe pattern captured by CCD, respectively, and the demodulated phase map can be seen in **Figure 14(f)**. As it can be seen from **Figure 14(e)** and (f), a pretty good phase map that is very close to the spherical phase profile is obtained. Comparing the results before and after static aberration compensation, it is evident that the static aberration compensation significantly improves the quality of the reconstructed spherical wavefront, which further demonstrates that the back panel curvature (static aberration) has been compensated effectively.

#### 4. Conclusion and discussion

To improve the phase control accuracy of LC-SLM, two factors, nonlinear response, and static aberration are comprehensively studied. A phase calibration method based on the self-generated grating by LC-SLM is introduced. Because of the common path configuration, the self-interference method can accurately obtain a phase modulation curve. Besides, a random phase-shifting interferometry is

introduced to measure the static aberration of a reflective SLM. With the help of phase calibration and static aberration compensation, the quality of the reconstructed wavefront by LC-SLM is greatly improved. However, other factors (such as pixel cross talk, internal Fabry–Perot cavity, fill factor, bit depth, phase flicker) also affect the phase control accuracy. A plenty of researchers have proposed some method to compensate the effect of the pixel cross talk [45–48], the phase flicker [49–53]. Nevertheless, most previous works mainly focused on the compensation of one factor. Recently, Pushkina [54] established a comprehensive model to compensate the effect of pixel cross talk, the back panel curvature (static aberration), and the internal Fabry-Perot cavity simultaneously. As a result, the performance of LC-SLM has been substantially improved. In general, different types of SLMs may have different optimized models. How to establish the optimal model for a specific LC-SLM by considering all the factors; and what is the best way to calibrate it? These are very interesting topics that need further research.



## Author details

Zixin Zhao  
Xi'an Jiaotong University, Xi'an, China

\*Address all correspondence to: [zixinzhao@xjtu.edu.cn](mailto:zixinzhao@xjtu.edu.cn)

## IntechOpen

© 2021 The Author(s). Licensee IntechOpen. This chapter is distributed under the terms of the Creative Commons Attribution License (<http://creativecommons.org/licenses/by/3.0>), which permits unrestricted use, distribution, and reproduction in any medium, provided the original work is properly cited. CC BY

## References

- [1] Chao L, Mingliang X, Quanqun M, et al. High-precision open-loop adaptive optics system based on LC-SLM. *Optics Express.* 2009;17(13):10774-10781. DOI: 10.1364/OE.17.010774
- [2] Kuang Z, Perrie W, Leach J, Sharp M, Edwardson SP, Padgett M, et al. High throughput diffractive multi-beam femtosecond laser processing using a spatial light modulator. *Applied Surface Science.* 2008;255(5p1):2284-2289. DOI: 10.1016/j.apsusc.2008.07.091
- [3] Justo A, Vicente D, Zbigniew J, et al. Measurement and compensation of optical aberrations using a single spatial light modulator. *Optics Express.* 2007; 15(13):15287-15292. DOI: 10.1364/OE.15.015287
- [4] Lazarev G, Chen P-J, Strauss J, Fontaine N, Forbes A. Beyond the display: Phase-only liquid crystal on Silicon devices and their applications in photonics [Invited]. *Optics Express.* 2019;27(11):16206-16249. DOI: 10.1364/oe.27.016206
- [5] Soutar C, Monroe SE, Knopp J. Complex characterization of the Epson liquid crystal television. *Proceedings of SPIE—The International Society for Optical Engineering.* 1959;1993:269-277. DOI: 10.1117/12.160293
- [6] Duffey JN, Jones BK, Loudin JA, Booth JJ. Optical characterization of the InFocus TVT-6000 liquid crystal television (LCTV) using custom drive electronics. *Proceedings of SPIE—The International Society for Optical Engineering.* 1995;275(4):2349-2358. DOI: 10.1117/12.205778
- [7] Bergeron A, Gauvin J, Gagnon F, Gingras D, Doucet M. Phase calibration and applications of a liquid-crystal spatial light modulator. *Applied Optics.* 1995;34(23):5133-5139. DOI: 10.1364/AO.34.005133
- [8] Zhang H, Zhang J, Wu L. Evaluation of phase-only liquid crystal spatial light modulator for phase modulation performance using a Twyman-Green interferometer. *Measurement Science & Technology.* 2007;18(6):1724-1728. DOI: 10.1088/0957-0233/18/6/S09
- [9] Wu Y, Nie J, Shao L. Method to measure the phase modulation characteristics of a liquid crystal spatial light modulator. *Applied Optics.* 2016; 55(31):8676-8682. DOI: 10.1364/AO.55.008676
- [10] Dai Y, Antonello J, Booth MJ. Calibration of a phase-only spatial light modulator for both phase and retardance modulation. *Optics Express.* 2019;27(13):17912-17926. DOI: 10.1364/oe.27.017912
- [11] Mukhopadhyay S, Sarkar S, Bhattacharya K, Hazra L. Polarization phase shifting interferometric technique for phase calibration of a reflective phase spatial light modulator. *Optical Engineering.* 2013;52(3):5602. DOI: 10.1117/1.OE.52.3.035602
- [12] Jeffrey A. Davis. Transmission and phase measurement for polarization eigenvectors in twisted-nematic liquid crystal spatial light modulators. *Optical Engineering.* 1998;37(11):3048-3052. DOI: 10.1117/1.601976
- [13] Reichelt S. Spatially resolved phase-response calibration of liquid-crystal-based spatial light modulators. *Applied Optics.* 2013;52(12):2610-2618. DOI: 10.1364/ao.52.002610
- [14] Wang H, Dong Z, Fan F, Feng Y, Lou Y, Jiang X. Characterization of spatial light modulator based on the phase in Fourier domain of the hologram and its applications in coherent imaging. *Applied Sciences.* 2018;8(7):1146. DOI: 10.3390/app8071146

- [15] Yang L, Xia J, Chang C, Zhang X, Yang Z, Chen J. Nonlinear dynamic phase response calibration by digital holographic microscopy. *Applied Optics*. 2015;54(25):7799-7806. DOI: 10.1364/AO.54.007799
- [16] Li R, Gao Y, Cao L. In situ calibration for a phase-only spatial light modulator based on digital holography. *Optical Engineering*. 2020;59(5):053101. DOI: 10.1117/1.OE.59.5.053101
- [17] Tiwari V, Gautam SK, Naik DN, Singh RK, Bisht NS. Characterization of a spatial light modulator using polarization-sensitive digital holography. *Applied Optics*. 2020;59(7):2024-2030. DOI: 10.1364/AO.380572
- [18] Engstrom D, Milewski G, Bengtsson J, Galt S. Diffraction-based determination of the phase modulation for general spatial light modulators. *Applied Optics*. 2006;45(28):7195-7204. DOI: 10.1364/AO.45.007195
- [19] Zhang Z, Yang H, Robertson B, Redmond M, Pivnenko M, Collings N, et al. Diffraction based phase compensation method for phase-only liquid crystal on silicon devices in operation. *Applied Optics*. 2012;51(17):3837-3846. DOI: 10.1364/AO.51.003837
- [20] Mendoza-Yero O, Mínguez-Vega G, Martínez-León L, Carbonell-Leal M, Fernández-Alonso M, Doate-Buendía C, et al. Diffraction-based phase calibration of spatial light modulators with binary phase fresnel lenses. *Journal of Display Technology*. 2016;12(10):1027-1032. DOI: 10.1109/JDT.2016.2580902
- [21] Ronzitti E, Guillon M, de Sars V, Emiliani V. LCoS nematic SLM characterization and modeling for diffraction efficiency optimization, zero and ghost orders suppression. *Optics Express*. 2012;20(16):17843-17855. DOI: 10.1364/OE.20.017843
- [22] Goodman JW. *Introduction to Fourier Optics*. 3rd ed. Greenwood Village: Roberts & Company Publishers; 2005
- [23] Li Y, Li Y, Zhang J, Li Y, Wang Z, Yin C, et al. Generalized phase calibration method of liquid crystal spatial light modulator with absolute reference system of obnoxious background light. *Optics and Lasers in Engineering*. 2020;132:106132. DOI: 10.1016/j.optlaseng.2020.106132
- [24] Bondareva AP, Cheremkhin PA, Evtikhiev NN, Krasnov VV, Starikov RS, Starikov SN. Measurement of characteristics and phase modulation accuracy increase of LC SLM "HoloEye PLUTO VIS". *Journal of Physics Conference*. 2014;536:012011. DOI: 10.1088/1742-6596/536/1/012011
- [25] Yang Y, Li Y, Li Y, Zhang J, Zhang Y, Liu D, et al. Calibration of phase liquid crystal spatial light modulators using high-order Taiji radial-shearing interferometry. *Laser Physics*. 2020;30(2):025003. DOI: 10.1088/1555-6611/ab5e22
- [26] Fuentes JLM, Fernández EJ, Prieto PM, Artal P. Interferometric method for phase calibration in liquid crystal spatial light modulators using a self-generated diffraction-grating. *Optics Express*. 2016;24(13):14159-14171. DOI: 10.1364/OE.24.014159
- [27] Zhao Z, Xiao Z, Zhuang Y, Zhang H, Zhao H. An interferometric method for local phase modulation calibration of LC-SLM using self-generated phase grating. *Review of Scientific Instruments*. 2018;89(8):083116. DOI: 10.1063/1.5031938
- [28] López-Quesada C, Andilla J, Martín-Badosa E. Correction of aberration in holographic optical tweezers using a Shack-Hartmann sensor. *Applied Optics*. 2009;48(6):1084-1090. DOI: 10.1364/AO.48.001084

- [29] Hart NW. Characterizing static aberrations in liquid crystal spatial light modulators using phase retrieval. *Optical Engineering*. 2007;46(8): 086601. DOI: 10.1117/1.2767258
- [30] Xiao C, Zhiguang S, Xiaotian C, et al. Backplane aberration calibration of spatial light modulators using a phase-retrieval algorithm. *Applied Optics*. 2016;55(31):8916-8924. DOI: 10.1364/ao.55.008916
- [31] Jesacher A, Schwaighofer A, Fürhapter S, Maurer C, Bernet S, Ritsch-Marte M. Wavefront correction of spatial light modulators using an optical vortex image. *Optics Express*. 2007; 15(9):5801-5808. DOI: 10.1364/OE.15.005801
- [32] Harriman JL, Linnenberger A, Serati SA, Ginglewski JD, Gruneisen MT, Giles MK. Improving spatial light modulator performance through phase compensation. *Proceedings of SPIE—The International Society for Optical Engineering*. 2004; 5553:58-67. DOI: 10.1117/12.563394
- [33] Zeng Z, Li Z, Fang F, Zhang X. Phase compensation of the non-uniformity of the liquid crystal on silicon spatial light modulator at pixel level. *Sensors*. 2021;21(3):967. DOI: 10.3390/s21030967
- [34] He A, Quan C. Wavefront correction for spatial nonuniformity of the liquid crystal on silicon based spatial light modulator. *Optics and Lasers in Engineering*. 2019;121:377-388. DOI: 10.1016/j.optlaseng.2019.05.010
- [35] Xu J, Qin S, Liu C, Fu S, Liu D. Precise calibration of spatial phase response nonuniformity arising in liquid crystal on silicon. *Optics Letters*. 2018; 43(12):2993-2996. DOI: 10.1364/OL.43.002993
- [36] Szatkowski M, Popiołek Masajada A, Masajada J. Optical vortex trajectory as a merit function for spatial light modulator correction. *Optics and Lasers in Engineering*. 2019;118:1-6. DOI: 10.1016/j.optlaseng.2019.01.014
- [37] Sheng Y, Zhou C, Yu C, Lai X, Wei K, Fan S, et al. Correction for the inherent aberration of liquid crystal spatial light modulator. *Holography, Diffractive Optics, and Applications*. 2018;10818:1081827. DOI: 10.1117/12.2502217
- [38] Arias A, Castaneda R. Estimation and Compensation of aberrations in Spatial Light Modulators. *Journal of Physics: Conference Series*. 2011;274(1): 012060. DOI: 10.1088/1742-6596/274/1/012060
- [39] Xun X, Cohn RW. Phase calibration of spatially nonuniform spatial light modulators. *Applied Optics*. 2004; 43(35):6400. DOI: 10.1364/AO.43.006400
- [40] Gongjian Z, Man Z, Yang Z. Phase modulation characteristics of spatial light modulator and the system for its calibration. *Journal of Electrical Engineering*. 2018;6(4):193-205. DOI: 10.17265/2328-2223/2018.04.001
- [41] McDermott S, Li P, Williams G, Maiden A. Characterizing a spatial light modulator using ptychography. *Optics Letters*. 2017;42(3):371-374. DOI: 10.1364/OL.42.000371
- [42] Li J, Zhao Z, Fan C, Du Y, Zhou M, Zhang X, et al., editors. Characterizing static aberration in reflective liquid crystal spatial light modulators (LC-SLM) using random phase shifting interferometry. In: 2021 International Conference of Optical Imaging and Measurement (ICOIM); 27-29 Aug Xi'an. New York: IEEE; 2021. 2021. DOI: 10.1109/ICOIM52180.2021
- [43] Escobar MA, Estrada JC, Vargas J. Phase-shifting VU factorization for interferometry. *Optics and Lasers in*

Engineering. 2020;124:105797. DOI: 10.1016/j.optlaseng.2019.105797

[44] Zhao Z, Zhao H, Zhang L, Gao F, Qin Y, Du H. 2D phase unwrapping algorithm for interferometric applications based on derivative Zernike polynomial fitting technique. Measurement Science and Technology. 2015;26(1):017001. DOI: 10.1088/0957-0233/26/1/017001

[45] Jz A, Hla B, Xu LA. Reducing the crosstalk effect in phase-only spatial light modulators based on double-phase method. Optics Communications. 2020; 465:125595. DOI: 10.1016/j.optcom.2020.125595

[46] Simon M, Monika R-M, Gregor T. Model-based compensation of pixel crosstalk in liquid crystal spatial light modulators. Optics Express. 2019; 27(18):25046-25063. DOI: 10.1364/OE.27.025046

[47] Guesmi M, Žídek K. Calibration of the pixel crosstalk in spatial light modulators for 4f pulse shaping. Applied Optics. 2021;60(25):7648-7652. DOI: 10.1364/AO.434309

[48] Chen Q, Shen X, Cheng Y, Liu J, Cai J, Liu Y. A crosstalk-reduced method of complex fields encoding using a single phase-only spatial light modulator. Optik. 2021;228:166190. DOI: 10.1016/j.ijleo.2020.166190

[49] Márquez A, Martínez-Guardiola FJ, Francés J, Gallego S, Pascual I, Beléndez A. Combining average molecular tilt and flicker for management of depolarized light in parallel-aligned liquid crystal devices for broadband and wide-angle illumination. Optics Express. 2019;27(4):5238-5252. DOI: 10.1364/oe.27.005238

[50] Moreno, Lizana, Márquez, Iemmi, Fernández. Time fluctuations of the phase modulation in a liquid crystal on silicon display: Characterization and

effects in diffractive optics. Optics Express. 2008;16(21):16711-16722. DOI: 10.1364/OE.16.016711

[51] Nobukawa T, Katano Y, Muroi T, Kinoshita N, Ishii N. Reduction of spatio-temporal phase fluctuation in a spatial light modulator using linear phase superimposition. OSA Continuum. 2021;4(6):1846-1858. DOI: 10.1364/OSAC.426628

[52] Yang Z, Wu S, Nie J, Yang H. Uncertainty in the phase flicker measurement for the liquid crystal on silicon devices. Photonics. 2021;8(8): 307. DOI: 10.3390/photonics8080307

[53] Zheng M, Chen S, Liu B, Weng Z, Li Z. Fast measurement of the phase flicker of a digitally addressable LCoS-SLM. Optik. 2021;242:167270. DOI: 10.1016/j.ijleo.2021.167270

[54] Pushkina A, Filho J, Maltese G, Lvovsky A. Comprehensive model and performance optimization of phase-only spatial light modulators. Measurement Science and Technology. 2020;31: 125202. DOI: 10.1088/1361-6501/aba56b